Final Technical Report

PI: Sergei Savikhin

Purdue University

Award number: DE-SC0001341

Revealing excitonic structure and charge transfer in photosynthetic proteins by time-resolved circular dichroism spectroscopy

S. Savikhin

Purdue University

Contents

1. Introduction.

While the general principles governing the light energy conversion in photosynthetic processes are well understood, there is a number of questions that remain open in spite of extensive experimental and theoretical work in that area. For example, there is still no agreement about the details of the primary charge separation and its dynamics in type I reaction centers (RC) – such as RC of photosystem I (PS I RC). The major problem here is posed by a large number of antenna pigments, which leads to spectral congestion and prevents the direct detection of the dynamics of cofactors involved in the process by optical means offered by modern time-resolved ultrafast techniques such as femtosecond (fs) pump-probe spectroscopy, fluorescence time measurements and coherent two-dimensional spectroscopy. Information about these ultrafast processes is usually obtained by fitting the optical signals observed in experiments with predefined energy/electron transfer models, and the results are, therefore, dependent on the model. The spectral and temporal selectivity of the conventional pump-probe spectroscopy are not able to distinguish the signals arising from the few pigments involved in electron transfer in a system as large as photosystem I. We proposed the addition of an extra "dimension" into the conventional pump-probe setup – namely we will introduce the ability to differentiate optical signals originating from the system not only by their spectral and temporal signatures, but also based on the circular dichroism (CD) properties of the molecules involved in energy and electron transfer.

The TRCD spectroscopy will also add a new dimension in the studies of other strongly coupled pigment-protein systems; in particular, we have applied it to study the Fenna Matthews Olson (FMO) complex. In spite of being thoroughly studied by means of steady-state spectroscopy and femtosecond (fs) spectroscopy (including two-dimensional electronic spectroscopy, 2DES), the spectral congestion has so far prevented definite and unambiguous assignment of the individual pigment site energies. As a result, a number of different Hamiltonians have been proposed to model properties of the FMO complex. Unlike conventional (transient) absorption, which is sensitive to the dot-products of the dipole transition moments of the interacting molecules, the CD signals sense their cross-products and are more sensitive to the structure. Our TRCD data obtained in the period of this grant proves that transient CD signals accompanying triplet energy transfer in the FMO can readily differentiate between these Hamiltonians (paper in preparation). The FMO complex, as one of the most thoroughly studied strongly coupled pigment-protein complexes, is an ideal test ground for the development of computational methods capable of predicting optical properties of photosynthetic complexes from first principles, and proposed experimental refinement of its properties will be accompanied and enhanced by molecular modeling.

Introduction of TRCD technique to photosynthetic studies has the potential to add a new angle to studies of many other systems that contain strongly coupled light absorbing molecules. Moreover, the TRCD technique will also be sensitive to conformational changes of proteins that are known to have a strong CD response in the UV-blue spectral region.

In this Technical Report we will describe two TRCD setups developed and built during this grant, one capable of resolving CD dynamics in nanosecond-to-millisecond time range, and another capable of femtosecond resolution. We will also introduce the results obtained so far for

FMO complex using nanosecond TRCD spectrometer and describe quantum-mechanical computational methods to model TRCD signals in both nanosecond and femtosecond regimes.

2. TRCD spectrometers

Time-resolved circular dichroism (TRCD) spectroscopy has been shown to have great potential for investigation of three-dimensional structural evolution during the reactions of biomolecules and chiral-chemical species. However, TRCD experiments (see some representative values in Table 1) have thus far been limited to species with strong CD signals such as myoglobin and Ruthenium blue dimer (Δ− and Λ− $Ru(bpy)_3^{+2}$) due to low sensitivity[2, 6-8 9, 10].

Table I: Time resolution and typical noise level for some representative TRCD schemes published earlier and in this work

Time resolution	dA_{CD} noise	work
1 ms	$2x10^{-4}$	Ferrone 1974[13]
0.4 ms	$6x10^{-4}$	Anson and Bayley 1974[10,11]
1 μs	$1x10^{-5}$	Mendonca 2014[25]
100 ns	$2x10^{-4}$	Shapiro 1995[26]
50 ns	$6x10^{-5}$	Lewis 1985[6]
20 ns	$1x10^{-4}$	Bjorling 1992[7]
2 ns	$5x10^{-3}$	Wen 1996[15]
1 ps	$1x10^{-4}$	Niezborala 2006[20]
250 fs	$1x10^{-4}$	Trifonov 2010[27]
150 fs	$1x10^{-4}$	Mangot 2010[28]
2.5 ps	$5x10^{-5}$	Hiramatsu 2015[29]
5 ns (scalable to fs range)	**$7x10^{-7}$**	**This work**
<100 fs	**$<10^{-8}$**	**This work**

Note, that expected TRCD signals for typical photosynthetic complexes like FMO are expected in the order of 10^{-5}, and none of the previously proposed methods was able to detect such low signals.

2.1. Nanosecond TRCD spectrometer

The TRCD spectrometer developed by our group uses an ellipsometric method to measure ΔA_{CD} following a general approach described, for example, by Lewis et al. [2] Similar approach has been used by a number of other groups, see, for example, [11-15] and a full review in our paper[3]. However, the reported noise level of these setups was ~$5x10^{-5}$ or larger in ΔA_{CD} (in OD units, See Table 1), not sufficient for the proposed study. To overcome that barrier, our design introduced a number of critical modifications, such as 3-channel light detection, and elimination of signal errors by solving the system of

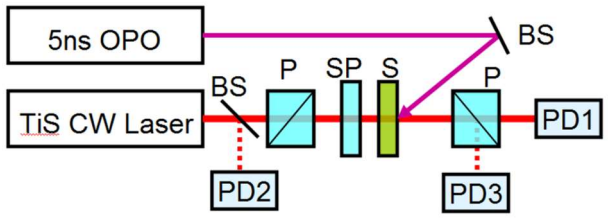

Fig.2.1.1. A simplified block diagram of the TRCD spectrometer built by PI. P-polarizer, SP-stress plate, S-sample, PD – fast photodiodes. See [3] for detailed description.

mathematical equations describing ΔA_{CD} exactly (without approximations). As a result, the sensitivity of the nanosecond TRCD spectrometer reached $<10^{-6}$ in ΔA_{CD} (<30 μdeg). Figure 2.1.1 depicts a simplified block diagram of the spectrometer; a detailed description is now published in [3]. Figure 2.1.2 (A,B) shows ordinary absorption differences ΔA and accompanying ΔA_{CD} transients measured for *triplet* energy transfer in the FMO complexes at room temperature. Panel C depicts typical noise spans in past TRCD realizations [2] plotted in the same scale as panel B. Note that *singlet* energy transfer occurs in femtosecond-to-picosecond time scale and cannot be resolved by that setup.

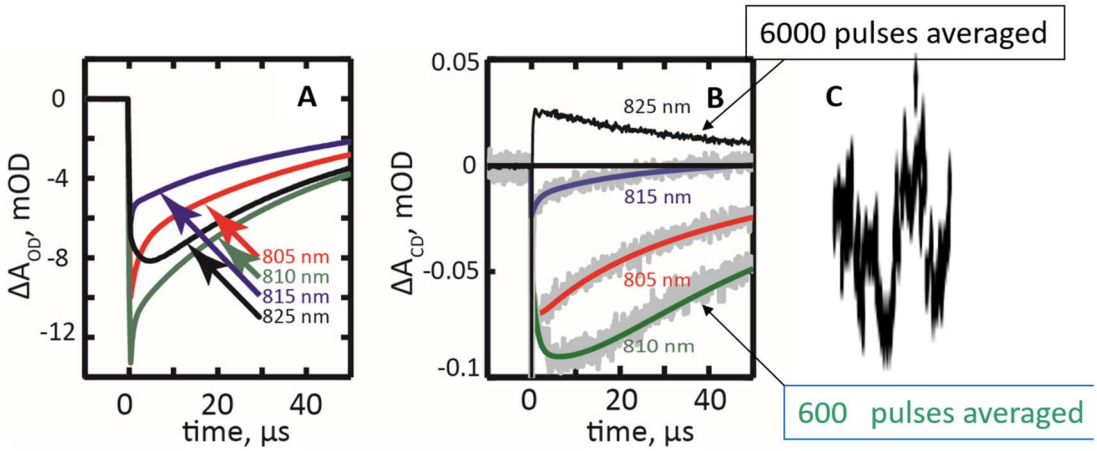

Fig.2.1.2. ΔA (**A**) and ΔA_{CD} (**B**) kinetics of the FMO at RT probed at shown wavelengths using the TRCD spectrometer built by PI. (**C**) typical noise span in ΔA_{CD} achieved in past realizations of TRCD setups (from [2], see more examples in [3]). ΔA and ΔA_{CD} are measured simultaneously in the same scan. The noise in (A) is smaller than the line thickness. Smooth lines in (B) show fits to ΔA_{CD} kinetics.

2.2. Femtosecond TRCD spectrometer

The ellipsometric approach described in for nanosecond TRCD can be used in the femtosecond (fs) regime by replacing pump and probe beams with tunable outputs of fs optical parametric amplifiers pumped by an amplified Ti:Sapphire laser. We verified this approach by converting our existing amplified fs pump-probe spectrometer into TRCD using the scheme similar to Fig. 1 and achieving sensitivity on-par with that of our nanosecond TRCD spectrometer. The drawback of the ellipsometric approach is, however, its inability to use CD-modulated beam as a pump beam, which is at the center of our proposal on PS I RC studies.

Measurements of TRCD signals using probe beam modulated between full left and right circular polarization have been performed in the past (for example: [9, 14-16]), and even applied to detect CD transients in bacterial RC[14]. However, the sensitivity of these setups has been insufficient for our purposes – for example, the measured ΔA_{CD} signals in case of bacterial RC were ~0.005 (in OD units), accompanied with ΔA~0.5. This would not be possible for PS I RC where, to achieve annihilation-free regime (i.e. 1 excitation per complex) signals must be >100 times smaller. It has been also recently demonstrated that CD signals in that regime can be detected using a fs pump-probe spectrometer variant [9], but the reported sensitivity was ~10^{-3}. An alternative design based

on 2DES technique was also recently realized[10], but its sensitivity could not be directly compared with more traditional TRCD designs as data were plotted in arbitrary units.

We have been working on building a fs TRCD setup using an alternative design based on the PI's ultra-sensitive pump-probe spectrometer that uses a fs Ti:Sapphire laser and double beam modulation at radiofrequency [17]. The use of the broadband output of a Ti:Sapphire laser allows for two-color fs pump-probe spectroscopy with pump and probe separated by 40 nm or more, as shown earlier by PI [18-24]. The radio-frequency (rf) modulation of both pump and probe beams and sideband detection technique results in the ΔA noise levels ~10^{-7} that make it very well suited for TRCD. In addition, the amplitude pump beam modulation can be replaced with CD modulation, making that setup ideally suited for PS I charge separation studies and similar tasks where the pump beam should selectively excite CD features in an otherwise congested spectrum.

A simplified diagram of the double beam rf modulation TRCD built by PI is shown in Fig. 2.2.1. The 20 fs pulses are generated by a dedicated home-built mode-locked Ti:Sapphire laser operating at a repetition rate of 80 MHz and tunable over the spectral range ~685-900 nm. The beam is split into pump and probe using a beam splitter BS. In the original pump-probe scheme [17] intensities of each beam were modulated at 6.5 MHz and 0.5 MHz, respectively, using acousto-optical modulators (AOM). The pump-probe ΔA signal was detected at the sum frequency 7 MHz using a special ultra-sensitive resonant photodiode detector developed by PI. In the first attempt to build a TRCD spectrometer we used a fast electro-optical CD modulator (EOM) since that required only a replacement of one of the AOMs with EOM. Unfortunately, EOM introduced significant additional noise into the beam degrading the sensitivity of this TRCD beyond acceptable limit. Instead, the new design of TRCD relies on a photoelastic modulator (PEM) for CD modulation. A number of challenging changes had to be introduced into existing dual-modulation pump-probe spectrometers to make it compatible with the fixed 50 kHz modulation frequency of PEM, which is set by the intrinsic acoustic resonance frequency of the PEM plate. In the new design the second beam is amplitude-modulated at 950 kHz, and the transient signals are measured at the sum frequency 1MHz – the region where the relative Ti:Sapphire output noise level falls below 10^{-8} $Hz^{-1/2}$. A special electronic driver had to be designed and built to provide the additional 950 kHz feed for AOM and the 1MHz reference output phase-

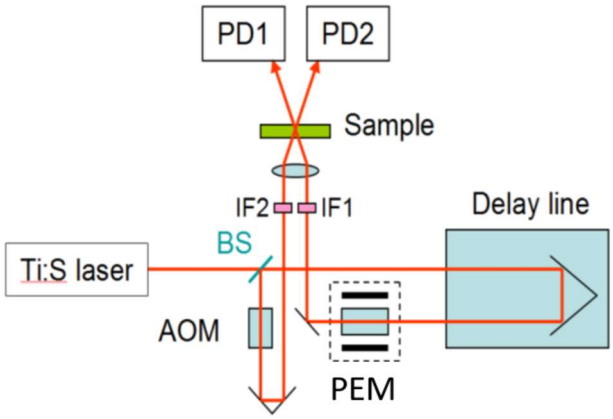

Fig.2.2.1. A simplified diagram of the femtosecond TRCD spectrometer proposed by PI. BS-beam splitter, PEM-CD modulator, AOM- intensity modulator, PD-photodiode

locked to the sum of the 50 kHz and 950 kHz drives. Close proximity of the sum frequency to the 950 kHz puts strict requirements on the sum-frequency mixing circuitry, since the 950 kHz signal level has to be $<10^{-8}$ of the sum frequency level in the reference channel (and vice versa). A new resonant photodetector also had to be built to address the change in the signal frequency. The close proximity of 950 kHz to the 1MHz resonant frequency also required special circuitry to filter out the 950 kHz before processing the signal in the lock-in amplifier. It was also discovered that the reflective optics used in the pump-probe spectrometer can result in additional amplitude modulation of the CD-modulated beam. To keep that modulation well below 10^{-3} (i.e. below the ratio of $\Delta A_{CD}/\Delta A$ for FMO, Fig. 2.1.3), several modifications are currently introduced to the original optical layout of the pump-probe scheme.

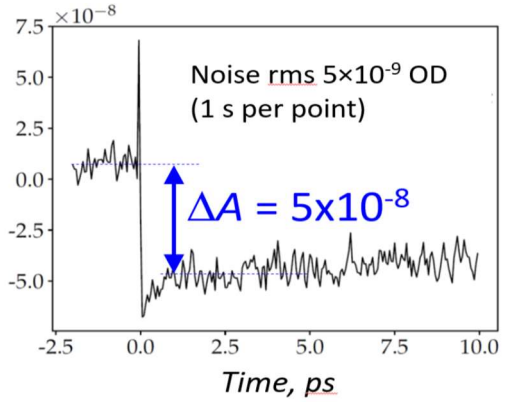

Fig.2.2.2. The sensitivity of the newly built femtosecond TRCD spectrometer with dual beam amplitude modulation measured with a test sample (laser dye IR140 in MeOH.

Fig. 2.2.2 shows a test measurement of an IR140 dye sample using the new spectrometer in dual-beam amplitude modulation regime demonstrating nearly shot-noise limited noise rms $<10^{-8}$. Fig. 2.2.3 shows the first measurements of ΔA_{CD} and ΔA in the FMO complex under the same excitation conditions using 1 second signal averaging time per point (a slight bimodal shape at $t=0$ is due to a chirp in the laser pulse; it will be compensated by a prism pair in the final setup). As expected, the two major kinetic components observed in that time span have similar decay times in ΔA and ΔA_{CD}, but their amplitude ratios are different. Note that at 790 nm both ΔA and ΔA_{CD} signals are expected to be relatively small, especially at longer delay times (see [18] and Fig. 2.1.3). While Fig. 2.3.3 clearly demonstrates that our new setup is capable of measuring TRCD signals in a photosynthetic protein, the noise level in ΔA_{CD} is higher than that in Fig. 2.2.3 for dual-beam amplitude modulation case. After careful investigation we found that this additional noise is caused by chaotic weak amplitude modulation that arises in the PEM probe beam after it is reflected from several mirrors between the PEM and the sample. We are currently redesigning the optical layout to eliminate any reflecting optics between PEM and the sample.

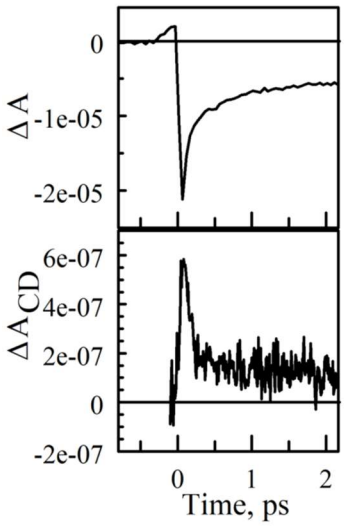

Fig.2.2.3. The first ΔA and ΔA_{CD} kinetics measured at RT with fs resolution in one-color pump-probe experiment at 790 nm for FMO complex.

A more detailed fs experimental diagram is depicted in Fig. 2.2.4 with most of the optical elements shown.

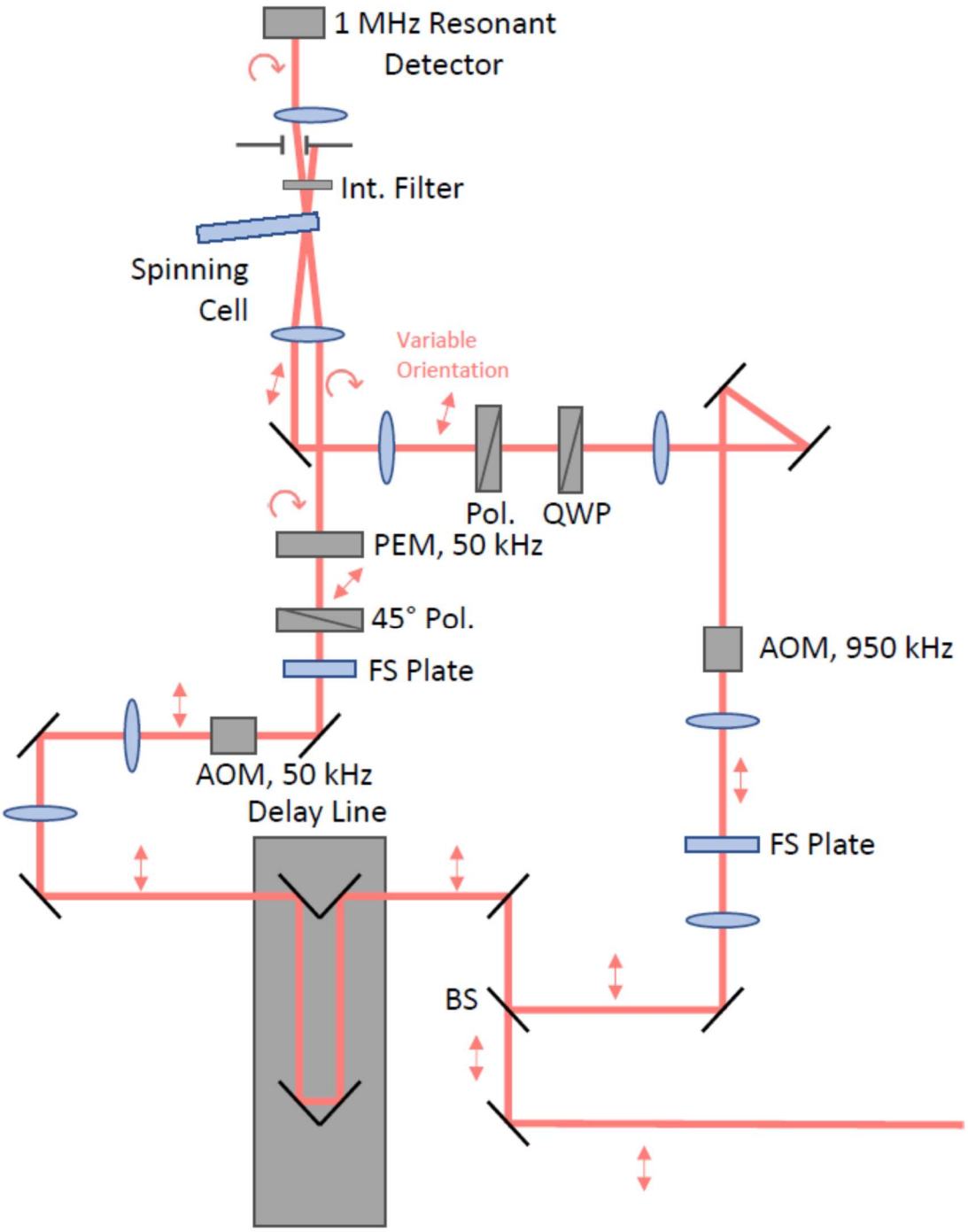

Fig. 2.2.4. Detailed block diagram of the femtosecond TRCD spectrometer. AOM – Acousto Optic light intensity Modulator; FS Plate – Fused silica plate, 45^0 Pol. – polarizer at 45^0 to horizontal; BS – beam splitter; QWP – quarter wave plate, Int. Filter – interference filter, spinning cell – round cell with the sample spinning at high speed to bring fresh sample into beam. Red line – fs light pulses delivered from home-built Ti:sapphire laser (not shown).

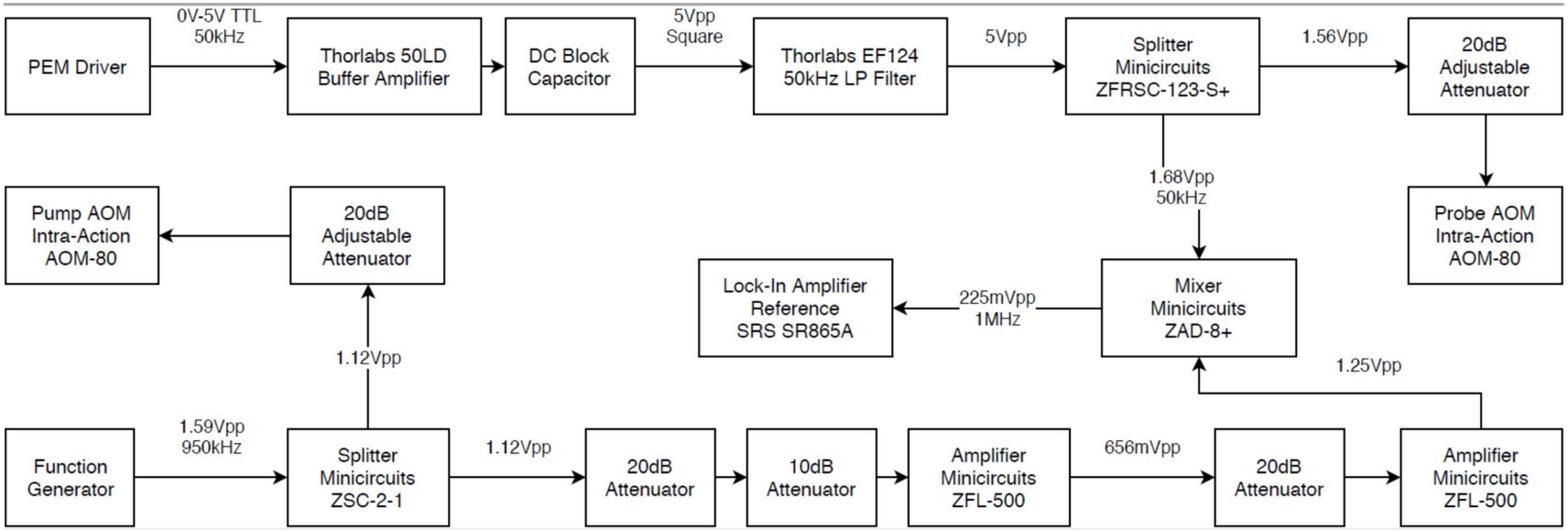

Fig. 2.2.5. Frequency driving schematics for dual-beam pump-probe modulation.

Driving electronics diagram is depicted in Figure 2.2.5. Note that isolation between the reference 1 MHz channel and the 50 kHz mudulated CD probe beam must be ~10^{-8} to detect weak CD signals. The isolation between 1 MHz channel and 950 kHz channel must better than 10^{-4} when CD-modulated beam is used as a probe, and 10^{-8} when it is used as a pump.

3. Theoretical background for pump-probe TRCD analysis

While computational modeling of conventional ΔA pump-probe signals obtained in excitonic systems has been developed earlier, the treatment of ΔA_{CD} has not been considered. In the report below we provide the extension of exciton theory to describe such signals.

3.1. Pump-probe signal decomposition

In pump-probe experiment the *pump* laser pulse promotes (fraction of) the excitonic complexes into excited state, and the second *probe* pulse interrogates absorption and circular dichroism (CD) differences caused by the pump pulse. Since it is a *difference* spectroscopy, only a sub-ensemble of excited complexes matters, and the changes in spectroscopic signals follow the dynamics of this sub-set of complexes.

In a limit of relatively low pump-probe intensities a single complex is excited just once. The changes in absorptivity (ΔA) and CD (ΔA_{CD}) can be modeled as a superposition of 3 components:

i) Photobleaching (PB), which arises due to the depletion of complexes in *ground* state, i.e. PB spectrum is equal to absorption spectrum of a complex in a ground state, but has an opposite sign since $\Delta A = A_{after\_pump} - A_{before\_pump}$. The signal is thus equal to: $\Delta A_{PB} = -(A_{before\_pump} \cdot N_{excited}/N_{total})$

ii) Excited State Absorption (ESA) arises due to emerging absorption of light by the fraction of excited complexes into higher excited states. For larger excitonic systems ESA signal is almost equal to the PB, but has an opposite sign, and the total ΔA will be defined by a *small* differences between PB and ESA. Assuming *n* equivalent pigments in one excitonic complex, PB ~ n, while ESA~(n-1).

iii) Stimulated Emission (SE) arises due to probe light induced transitions from complexes excited by the pump pulse back into ground state. It is always negative and its intensity is ~1 (defined by the dipole moment of currently excited state)

3.2. Photobleachaing (PB) spectrum

This is simply the absorption spectrum of complex in ground state. In case of an excitonic complex consisting of *n* coupled pigments excited states are delocalized over all pigments resulting in *n* excitonic states. The theory of steady-state absorption and CD spectra in a strongly coupled system is well described in "Photosynthetic Excitons" by H. Amerongen, L Valkunas and R van Grondelle, see Chapter 2.

Briefly, in the case of *n* oscillators (*n* coupled pigments in a complex), the properties of the system are described by the Hamiltonian of the system written in the form [25, 26]:

$$H = \sum_{p=1}^{n} \hat{H}_p + \sum_{p=1,n-1}^{n} \sum_{q=p+1}^{n} \hat{V}_{pq} \qquad (1)$$

where H_p is the electronic Hamiltonian for pigment p and V_{pq} represents the interaction energy between pigments p and q. The n singly excited delocalized excitonic states $\psi_i^{(1)}$ can be expanded in the (orthogonal) basis of n localized states $\chi_i^{(1)}$, where excitation is localized on the i^{th} pigment:

$$\left|\chi_i^{(1)}\right\rangle = \left|\varphi_1\varphi_2\cdots\varphi_i^*\cdots\varphi_n\right\rangle,\ i=1,2,\ldots,n \tag{2}$$

$$\left|\psi_i^{(1)}\right\rangle = \sum_{j=1,n} c_j^i \left|\chi_j^{(1)}\right\rangle \tag{3}$$

Here φ_i is a wave function of a pigment i in ground state, and φ_i^* represents that pigment in excited state.

In a similar way the (common) excitonic ground state is:

$$\left|\chi^{(0)}\right\rangle = \left|\varphi_1\varphi_2\cdots\varphi_i\ \cdots\varphi_n\right\rangle \tag{4}$$

The delocalized (excitonic) stationary states of the complex that are described by the Hamiltonian eq. 1 are obtained by solving the Schrödinger equation:

$$H\left|\psi_k^{(1)}\right\rangle = E_k\left|\psi_k^{(1)}\right\rangle = \sum_{i=1,n} c_i^k \left|\chi_i^{(1)}\right\rangle \tag{5}$$

In matrix representation, the matrix elements of the Hamiltonian can be easily inferred by substituting H from eq. 1 into 5. The diagonal elements correspond to the energies of the localized states H_i, and the off-diagonal matrix elements are interaction energies V_{ij}:

$$\begin{aligned} H_{ii} &= \left\langle \chi_i^{(1)} \mid \hat{H}_i \mid \chi_i^{(1)} \right\rangle \equiv H_i \\ H_{ij} &= \left\langle \chi_i^{(1)} \mid \hat{V}_{ij} \mid \chi_j^{(1)} \right\rangle \equiv V_{ij} \end{aligned} \tag{6}$$

In this formalism, the problem of finding the excitonic transitions is mathematically equivalent to diagonalization of the above Hamiltonian matrix [27]. The n eigenvalues found by H matrix diagonalization correspond to the energies E_i of the excitonic levels, while the respective eigenvectors c_j^i represent expansion coefficients of the (excited) excitonic wave function, $\psi_i^{(1)}$, as follows:

$$\left|\psi_i^{(1)}\right\rangle = \sum_{j=1}^{n} c_j^i \left|\chi_j^{(1)}\right\rangle \tag{7}$$

Thus, the coefficients $|c_j^i|^2$ represent the yield of chromophore j in the excitonic transition at energy E_i, i.e. characterize the delocalization of excitation over n pigments.

Interaction of individual molecular transition with EM field of light is described by the transition dipole moment $\vec{\mu}_i$:

$$\begin{aligned} \vec{\mathcal{E}}_0 \cdot \vec{\mu}_i &= \vec{\mathcal{E}}_0 \cdot \left\langle \varphi_i^* \mid \hat{\mu}_i \mid \varphi_i \right\rangle \\ \vec{\mu}_i &= \left\langle \varphi_i^* \mid \hat{\mu}_i \mid \varphi_i \right\rangle \end{aligned} \tag{8}$$

where $\vec{\mathcal{E}}_0$ is oscillating electric field amplitude and $\hat{\mu}$ is a dipole moment operator. The absorption strength is thus $\sim\left|\vec{\mu}_i\right|^2$.

The singly excited excitonic transition dipole moment, $\eta_i^{(1)}$, can be then expressed as a superposition of transition moments of individual non-interacting pigments, μ_j, over which excitation is delocalized:

$$\begin{aligned}
&\vec{\eta}_i^{(1)} = \left\langle \psi_i^{(1)} \mid \hat{\mu} \mid \psi_i^{(0)} \right\rangle = \left\langle \sum_{j=1}^{n} c_j^i \chi_j^{(1)} \mid \hat{\mu} \mid \varphi_1 \varphi_2 \cdots \varphi_i \ \cdots \varphi_n \right\rangle \\
&\hat{\mu} = \sum_{i=1}^{n} \hat{\mu}_i \\
&\vec{\eta}_i^{(1)} = \sum_{j=1}^{n} c_j^i \left\langle \varphi_1 \varphi_2 \cdots \varphi_j^* \cdots \varphi_n \mid \hat{\mu} \mid \varphi_1 \varphi_2 \cdots \varphi_j \cdots \varphi_n \right\rangle \\
&\vec{\eta}_i^{(1)} = \sum_{j=1}^{n} c_j^i \left\{ \left\langle \varphi_1 \mid \hat{\mu}_1 \mid \varphi_1 \right\rangle + \left\langle \varphi_2 \mid \hat{\mu}_2 \mid \varphi_2 \right\rangle + \cdots + \left\langle \varphi_j^* \mid \hat{\mu}_j \mid \varphi_j \right\rangle + \cdots + \left\langle \varphi_n \mid \hat{\mu}_n \mid \varphi_n \right\rangle \right\}
\end{aligned} \tag{9}$$

Which results in a simple expression for excitonic transition dipole moment:

$$\vec{\eta}_i^{(1)} = \sum_{j=1}^{n} c_j^i \vec{\mu}_j \tag{10}$$

The optical absorption is described by n excitonic absorption bands at energies E_i, each having oscillator strength $|\eta_i|^2$. The direction of the transition vectors $\vec{\eta}_i$ defines the *linear* dichroism of the system. Thus, modeling PB signal is a task of writing down Hamiltonian matrix as outlined in eq. 6 and diagonalizing this Hamiltonian, the obtained eigenvalues E_i will correspond to transition energy of each excitonic band, and absorption strength of each respective band could be found by squaring the excitonic transition dipole moment (eq. 10). Note that diagonal elements H_{ii} of the matrix correspond to transition energies of respective *noninteracting* pigments, and off-diagonal elements H_{ij} represent interaction between pigments i and j. In the case of singlet excitations couplings between pigments are typically dominated by the resonance dipole-dipole interactions:

$$V_{ij} = \frac{\vec{\mu}_i \bullet \vec{\mu}_j - 3(\vec{\mu}_i \bullet \hat{r})(\vec{\mu}_j \bullet \hat{r})}{r^3} \tag{11}$$

where r is the center-to-center distance between the pair of interacting pigments, and $\hat{r}$ is the unit vector in the direction from pigment i to pigment j.

Circular dichroism – PB component. In the case of flat molecules, such as chlorophylls, there is no intrinsic circular dichroism, since intrinsic dichroism relies on coupling between magnetic and electric dipoles of a molecule. While the circular current can be generated in a π-orbital system of flat Chl molecule, the respective induced magnetic dipole is perpendicular to the plain, while electric transition dipole lays in the plane of the molecule, and the resulting dot product between the two results in 0.

However, the coupled system of such pigments can have a significant CD since an excitonic band is a collective (delocalized) transition of multiple pigments with μ's facing in different direction and *separated by a significant distance*. The transition probability is defined by the product of electric field and transition dipole moment:

$$\left|\vec{\mathcal{E}}\left(\vec{r}\right)\cdot\vec{\eta}_i^{(1)}\right|^2=\left|\sum_{j=0,n}\vec{\mathcal{E}}\left(\vec{r}_j\right)\cdot c_j^i\vec{\mu}_j\right|^2 \qquad (12)$$

where $\mathcal{E}$ is the optical electric field at position r of the chromophore. Due to the fact that for circularly polarized light the direction of electric field rapidly varies along the beam, the product in eq. 12 may and generally is different for RCL and LCL (right and left circularly polarized light), because dipoles μ_j are at different locations and electric field alignment with the dipole moment directions are not in phase for all pigments. The difference in absorptivity of RCD and LCD, or rotational strength of excitonic absorption band i can be expressed as (assuming the size of the excitonic system is << λ):

$$R_i=-\frac{\pi}{2\lambda}\sum_{k,j=1}^{n}c_k^ic_j^i\left[\vec{r}_{kj}\cdot\left(\vec{\mu}_k\times\vec{\mu}_j\right)\right] \qquad (13)$$

Where λ is wavelength of light and r_{ki} is a vector pointing from pigment k to pigment j. Note that depending on the orientation of molecules the cross product may be positive or negative. Note also that the sum of rotational strengths of all excitonic bands is exactly 0. For example, in a dimer the two bands in CD spectrum will be of opposite sign, but of the same magnitude, while the respective absorption bands may have different amplitudes.

Note, that in the case of multiple strongly coupled pigments the CD signal becomes more complex, but it remains being more sensitive to structural changes. The green lines in Figure 3.1 depict absorption and CD spectra of the FMO complex calculated by PI using the 7x7 Hamiltonian proposed by [1]. The blue lines correspond to the same Hamiltonian, except the (diagonal) energies of pigments #3 and #4 are swapped. Changes in the CD spectra associated with this swap are far more pronounced than changes in the absorption spectra.

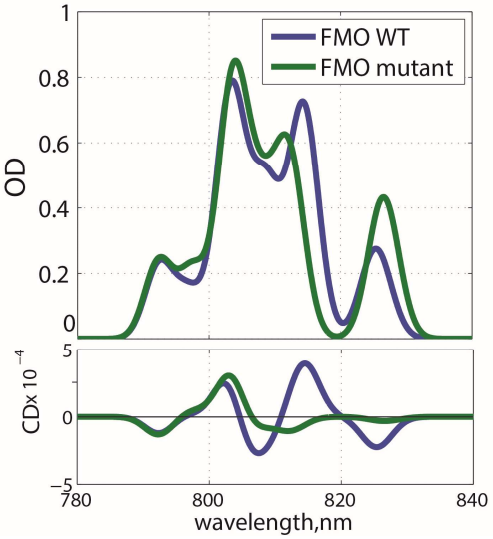

Fig.3.1. Absorption (top) and CD (bottom) calculated by PI using FMO Hamiltonian [1] as is (blue line) and with the pigment energies #3 and #4 swapped.

3.3. Excited State Absorption (ESA) spectrum: fs experiment (singlet states)

The excited state absorption in an excitonic system is not due to excitations to higher excited states of individual pigments (i.e. Soret band). The excited state absorption arises even in the case when each pigment constituting the complex has only one excited state. As a matter of fact, we will only take into account that one state, and ignore the higher excited states of each individual pigment.

To understand the physics behind the formation of ESA in excitonic state let us assume for a moment that there is (almost) no interactions between the pigments in the complex, i.e. all off-diagonal elements $H_{ij,i\neq j}$=0. Hamiltonian matrix is then diagonal and solving eq. 5 will then result

in *fully localized states*, i.e. $c_i^j = \delta_{ij}$, and $\left|\psi_i^{(1)}\right\rangle = \left|\chi_i^{(1)}\right\rangle$, $E_i = H_{ii}$. However, according to exciton theory, when we excite *any* state (which is just one pigment here) the PB spectrum is still a superposition of absorption of all pigments. On the other hand, removing one absorbing pigment in a noninteracting complex should leave the absorption bands of the remaining pigments intact, which is not the case if we only take into account PB. To remove this discrepancy, a 'doubly' excited excitonic state is constructed – since the complex's remaining n-1 pigments still absorb light their absorption is denotes as excitation from singly excited complex into doubly excited complex. In that simple noninteracting case the doubly excited complex means that in addition to the originally excited pigment, we can excite a second pigment (one of *n-1* that were still in ground state).

To consider a coupled system, we will now construct the delocalized two-excitonic states, and we will expand them in the basis of *n(n-1)/2* wave functions, where two of the pigments are excited simultaneously [25] as in the noninteracting case above:

$$\left|\chi_{ij}^{(2)}\right\rangle = \left|\varphi_1\varphi_2\cdots\varphi_i^*\cdots\varphi_j^*\cdots\varphi_n\right\rangle,\ i=1,\ldots,n-1,\ j=i+1,\ldots,n \tag{14}$$

The indices *i* and *j* are enumerated in such a way that each unique combination of two indices *ij* occurs only once (note that *ij* is also equivalent to *ji*). Note that, unlike Soret bands, these states cannot be observed in a steady state absorption, because going from ground state to doubly excited state would require to excite two pigments simultaneously and thus the photon energy of should split between two transitions with energies H_i and H_j. This is illustrated below for just one transition to one doubly excited localized state:

$$\vec{\mu}_{ij}^{(0\to 2)} = \left\langle\varphi_1\varphi_2\cdots\varphi_i^*\cdots\varphi_j^*\cdots\varphi_n\left|\hat{\mu}\right|\varphi_1\varphi_2\cdots\varphi_i\ \cdots\varphi_j\cdots\varphi_n\right\rangle$$

$$\vec{\mu}_{ij}^{(0\to 2)} = \left\langle\varphi_1\varphi_2\cdots\varphi_i^*\cdots\varphi_j^*\cdots\varphi_n\left|\sum_{k=1}^{n}\hat{\mu}_k\right|\varphi_1\varphi_2\cdots\varphi_i\ \cdots\varphi_j\cdots\varphi_n\right\rangle$$

$$\vec{\mu}_{ij}^{(0\to 2)} = \sum_{k=1}^{n}\left\langle\varphi_1\varphi_2\cdots\varphi_i^*\cdots\varphi_j^*\cdots\varphi_n\left|\hat{\mu}_k\right|\varphi_1\varphi_2\cdots\varphi_i\ \cdots\varphi_j\cdots\varphi_n\right\rangle$$

However, only these terms are non-zero:

$$\left\langle\varphi_i^*\left|\hat{\mu}_i\right|\varphi_i\right\rangle = \vec{\mu}_i \tag{15}$$

Thus, for term i, for example, we will have:

$$\left\langle\varphi_1\varphi_2\cdots\varphi_i^*\cdots\varphi_j^*\cdots\varphi_n\left|\hat{\mu}_i\right|\varphi_1\varphi_2\cdots\varphi_i\ \cdots\varphi_j\cdots\varphi_n\right\rangle =$$

$$= \left\langle\varphi_1\middle|\varphi_1\right\rangle\left\langle\varphi_2\middle|\varphi_2\right\rangle\cdots\left\langle\varphi_i^*\left|\hat{\mu}_i\right|\varphi_i\right\rangle\cdots\left\langle\varphi_j^*\middle|\varphi_j\right\rangle\cdots\left\langle\varphi_n\middle|\varphi_n\right\rangle =$$

$$= 1\cdot 1\cdots\bar{\mu}_i\cdots 0\cdots 1$$

And :

$$\vec{\mu}_{ij}^{(0\to 2)} = 0$$

The doubly excited states become significant only for transitions from singly excited states to the doubly excited states. For example, transition from localized singly excited state $\chi_i^{(1)}$ to state $\chi_{ij}^{(2)}$ gives us:

$$\begin{aligned}
\vec{\mu}_{i\to ij}^{(1\to 2)} &= \left\langle \varphi_1\varphi_2\cdots\varphi_i^*\cdots\varphi_j^*\cdots\varphi_n \middle| \hat{\mu} \middle| \varphi_1\varphi_2\cdots\varphi_i^*\cdots\varphi_j\cdots\varphi_n \right\rangle \\
\vec{\mu}_{i\to ij}^{(1\to 2)} &= \left\langle \varphi_1\varphi_1 \right\rangle \left\langle \varphi_2\varphi_2 \right\rangle \cdots \left\langle \varphi_i^*\varphi_i^* \right\rangle \cdots \left\langle \varphi_j^* \mid \hat{\mu}_j \mid \varphi_j \right\rangle \cdots \left\langle \varphi_n^*\varphi_n^* \right\rangle \\
\vec{\mu}_{i\to ij}^{(1\to 2)} &= \vec{\mu}_j \\
E_{i\to ij}^{(1\to 2)} &= H_j
\end{aligned} \tag{16}$$

The other point to notice in the above eq. is that in the optical $\chi_l^{(1)} \rightarrow \chi_{ij}^{(2)}$ transition the transition dipoles are zero when $l \neq i$ and $l \neq j$. It makes sense, since going from singly excited state l to doubly excited state ij require pigment l to go to ground state, and pigments i and j to go to excited state simultaneously upon absorbing a photon – a three-photon process of very low probability. If, however, pigment i is already excited, then going to doubly excited state ij is equivalent to exciting just one pigment j whose oscillator strength will define the respective transition dipole moment from $\chi_i^{(1)} \rightarrow \chi_{ij}^{(2)}$.

$$\begin{aligned}
\vec{\mu}^{i\to ij} &= \left\langle \chi_{ij}^{(2)} \mid \hat{\mu} \mid \chi_i^{(1)} \right\rangle = \left\langle \varphi_1\varphi_2\cdots\varphi_i^*\cdots\varphi_j^*\cdots\varphi_n \mid \hat{\mu} \mid \varphi_1\varphi_2\cdots\varphi_i^*\cdots\varphi_j\cdots\varphi_n \right\rangle \\
\vec{\mu}^{i\to ij} &= \left\langle \varphi_j^* \mid \hat{\mu}_j \mid \varphi_j \right\rangle = \vec{\mu}_j
\end{aligned} \tag{17}$$

Thus, the diagonal and non-zero off-diagonal elements of the Hamiltonian to describe the doubly excited excitonic states are given by

$$\begin{aligned}
\left\langle \chi_{ij}^{(2)} \middle| \hat{H} \middle| \chi_{ij}^{(2)} \right\rangle &= H_i + H_j \\
\left\langle \chi_{ij}^{(2)} \middle| \hat{H} \middle| \chi_{ik}^{(2)} \right\rangle &= \left\langle \chi_{ji}^{(2)} \middle| \hat{H} \middle| \chi_{ki}^{(2)} \right\rangle = V_{jk}, k \neq j
\end{aligned} \tag{18}$$

The off-diagonal elements, or interactions are nonzero only between states $\chi_{ik}^{(2)}$ and $\chi_{im}^{(2)}$ and between $\chi_{ik}^{(2)}$ and $\chi_{mk}^{(2)}$, i.e. between doubly excited states that have one common pigment in excited state. This reflects the fact that transitions are significant only between singly and doubly excited states, where just one more pigment is excited *in addition* to already excited pigment, and the interactions between these states are equal to interactions between these additional pigments. Thus the doubly excited Hamiltonian elements are completely defined by the elements of the singly excited one.

Diagonalization of the above Hamiltonian results in a set of eigenvalues (excitonic energies $E_i^{(2)}$) and eigenvectors $d_{(ij)}^k$; the two-exciton states, k, are linear combinations of the respective basis functions $\chi_{ij}^{(2)}$.

Note, that technically the indices ij for the doubly excited Hamiltonian is just a single counter in the respective matrix, each row and column is counted sequentially $k=1,\ldots(n(n-1)/2)$ and for each k we have a single unique doubly excited state defined by (i,j) pair. For example, let us build a Hamiltonian for doubly excited state of system of 4 pigments. The basis will have $n(n-1)/2=4(4-1)/2=6$ unique localized doubly excited states, where pairs of pigments 12, 13, 14, 23, 24, 34 are excited, respectively. The Hamiltonian:

Excited pigments	ij=1,2	1,3	1,4	2,3	2,4	3,4
1,2	H_1+H_2	V_{23}	V_{24}	V_{13}	V_{14}	0
1,3	V_{23}	H_1+H_3	V_{34}	V_{12}	0	V_{14}
1,4	V_{24}	V_{34}	H_1+H_4	0	V_{12}	V_{13}
2,3	V_{13}	V_{12}	0	H_2+H_3	V_{34}	V_{24}
2,4	V_{14}	0	V_{12}	V_{34}	H_2+H_4	V_{23}
3,4	0	V_{14}	V_{13}	V_{24}	V_{23}	H_3+H_4

(19)

Technically in a computer program, while building 6x6 Hamiltonian one should also build a translation table 6x2, where each of the 6 rows stores two numbers *i* and *j*. That will be needed to properly calculate the transition dipole moments.

The transition dipole moment of each ESA band due to the transition from the singly excited state *l* to the doubly excited state *k* can be then derived as follows:

$$\begin{aligned}\vec{\eta}^{(2)}_{l\to k} &= \left\langle \psi^{(2)}_k \,|\, \hat{\mu} \,|\, \psi^{(1)}_l \right\rangle \\ \vec{\eta}^{(2)}_{l\to k} &= \left\langle \sum_{(ij)}^{n(n-1)/2} d^k_{(ij)} \chi^{(2)}_{ij} \,|\, \hat{\mu} \,|\, \sum_{m=1}^{n} c^l_m \chi^{(1)}_m \right\rangle \\ \vec{\eta}^{(2)}_{l\to k} &= \sum_{(ij)}^{n(n-1)/2} \sum_{m=1}^{n} d^k_{(ij)} c^l_m \left\langle \chi^{(2)}_{ij} \,|\, \hat{\mu} \,|\, \chi^{(1)}_m \right\rangle\end{aligned} \tag{20}$$

In analogy with Eq. 17 one can see that the only nonzero matrix elements are the ones where excited pigment *m* in singly excited basis function $\chi^{(1)}_m$ is the same, as one of the excited pigments *i* or *j* in doubly excited basis $\chi^{(2)}_{ij}$:

$$\left\langle \chi^{(2)}_{ij} \,|\, \hat{\mu} \,|\, \chi^{(1)}_m \right\rangle = \vec{\mu}_j \delta_{im} + \vec{\mu}_i \delta_{jm} \tag{21}$$

And we end up with the following equation for the transition dipole moment from singly excited state *l* to doubly excited state *k*:

$$\vec{\eta}^{(2)}_{l\to k} = \sum_{(ij),m} d^k_{(ij)} c^l_m \left(\vec{\mu}_j \delta_{im} + \vec{\mu}_i \delta_{jm} \right) \equiv \sum_p f_{lkp} \vec{\mu}_p \tag{22}$$

This transition dipole moment is just a linear combination of transition moments of individual pigments; the coefficients f_{lkp} are cumulative expansion coefficients defined by (22).

The square $\left|\vec{\eta}^{(2)}_{l\to k}\right|^2$ yields oscillator strength of each of the doubly excited (n-1)n/2 states and the transition energies are given by the difference between eigenvalues $E^{(2)}$ and respective singly excited state energy $E^{(1)}{}_l$. Note that ESA spectrum depends on the singly excited state and thus may evolve in time if energy is transferred between singly excited states, while PB spectrum is static in shape.

The coefficients f_{lki} are instrumental in finding rotational strength of each of these transitions and they are expressed similarly to the singly excited states (eq. 13):

$$R^{(2)}_{l\to k} = -\frac{\pi}{2\lambda}\sum_{i,j}^{n} f_{lki} f_{lkj}\left[\vec{r}_{ij}\cdot\left(\vec{\mu}_i \times \vec{\mu}_j\right)\right] \qquad (23)$$

3.3. Excited State Absorption (ESA) spectrum: ns-µs experiment (triplet states)

Singlet exited states of chromophores are usually in the order of a nanosecond or shorter. Thus, in TRCD experiments at longer times the observed signals will be associated with long living (>100ns … 1 ms) triplet excited states. In the case of the FMO complex we have computed triplet-triplet interactions to be so weak that these excitations are almost fully localized on individual pigments. In this case the PB spectrum is still fully described by the equations in section 3.2.

The ESA spectra for triplet excited states can be *also* modeled using the computational strategy described in section 3.2 by deleting the pigment that is currently in triplet state from Hamiltonian eq. 6 and calculating absorption of the complex with one missing pigment

3.4. SE: stimulated emission

The stimulated emission is entirely defined by the oscillator strength of the individual singly excited exciton that is currently excited, i.e. by the square of transition dipole moment (eq. 10) and its rotational strength is given by eq. 13. It assumes that there is no dramatic change in the oscillator strength in excited state. One may introduce a stoke shift to the stimulated emission band as opposed respective absorption. Note that SE exists only for singlet excited states, and in the case of triplet excited state there is not SE component as the optical transition from triplet excited state to ground state is forbidden.

4. Nanosecond TRCD spectroscopy of the FMO complex

The FMO complex was the first photosynthetic pigment-protein complex resolved by X-ray crystallography by [4, 28] (Fig. 4.1) and it has since then been one of the most studied photosynthetic complexes [29, 30]. The FMO complex was the first pigment-protein complex for which quantum coherences and beatings between excitonic states were observed by PI in 1997 [31]. The study of excitonic structure and coherence in this complex led later to the development of a new technique – two-dimensional spectroscopy [1, 32-34]. Yet, there is

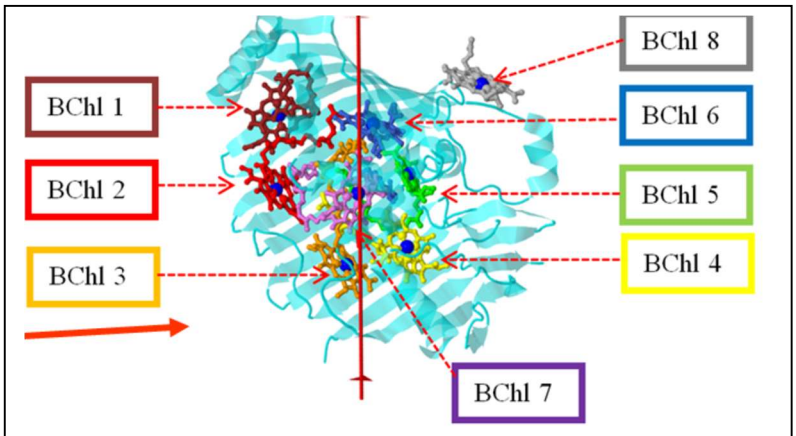

Fig.4.1. The structure of one subunit of FMO showing the locations of 8 BChl *a* molecules [4].

still a debate about the energies of the individual pigments in this system. This makes FMO the best candidate for the first application of TRCD in photosynthesis.

The FMO complex is a trimeric bacteriochlorophyll *a* (BChl *a*) protein complex that promotes electronic energy transfer from the light-harvesting antenna (chlorosome) to reaction centers in green sulfur bacteria [29, 30, 35]. Each of the three identical protein subunits of FMO encloses 7 BChl *a* pigments, with the 8th BChl *a* located between the subunits. The pigments 1-7 are closely spaced, leading to considerable excitonic interactions between them (up to ~200 cm^{-1}) [30]. The eighth pigment is not bound as strongly to the system, and consequently was overlooked in the first x-ray structures of the FMO complex (see [36] [37, 38] for details).

For the past three decades a number of different spectroscopic methods have been applied to study the FMO complex with an attempt to isolate the properties of individual pigments in the FMO complex (see review [30]). The optical properties of this complex are governed by excitonic couplings between the pigments and therefore BChl molecules generally cannot be excited or probed individually. As a result, the values of the site energies (H_i in eq. 6) of the BChls in FMO can be obtained only by modeling various optical properties of the FMO complex and about ten different sets of these diagonal energies have been proposed over the years (see, for example [1, 30, 33, 34, 39-41]). These values are crucial in modeling the properties and function of the complex. Note that the PI has modeled FMO in past using exciton models including effects of disorder [25, 31, 42-45].

The excitonic bands in the FMO complex overlap, resulting in only 3 major features in the absorption spectrum at low T. These features blend into one band at physiological room temperatures (Fig. 4.2). Conventional pump-probe and 2D spectroscopy can capture some extra features by observing spectral changes associated with excitation transfer between excitonic levels and coherence beats [43, 44] [1]. However, pump-probe signals, ΔA, are superposition of the PB spectrum (8 bands for 8 coupled pigments), and SE (1 band) with the ESA spectrum consisting of 28 bands. Interpretation of the resulting spectra is not a simple task and modeling does not result in a unique Hamiltonian.

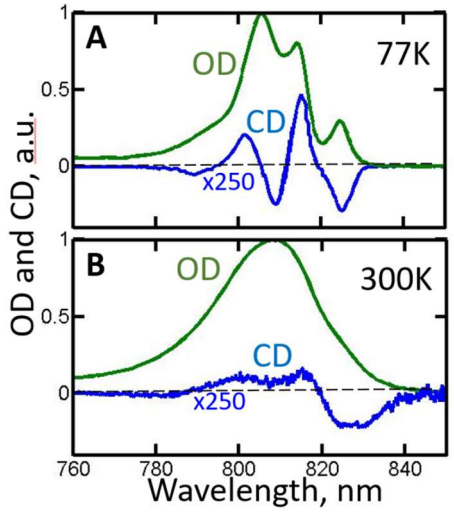

Fig.4.2. Absorption and CD of FMO at 77K (A) and 300K (B) show that CD can resolve excitonic bands even at RT.

PI has shown that the information on the individual pigments in FMO can be accessed using *triplet state* dynamics [46] that occurs on nanosecond-microsecond time scale, as opposed to the femtosecond singlet exciton dynamics. Upon excitation, a fraction of excited complexes (up to 10%) ends up in a *triplet* excited state. Our exciton simulations show that *triplet* excitation is localized on a single pigment, unlike a delocalized singlet excited state. Thus, the ESA signal for triplet excitation corresponds to the excitonic absorption spectrum of the *remaining*, un-excited pigments, with only 7 bands. Essentially, the FMO complex in a triplet state is similar to a mutant missing one pigment,

with the rest of the structure largely unaffected, and the measured difference spectra reveal the properties of that pigment in a most direct way.

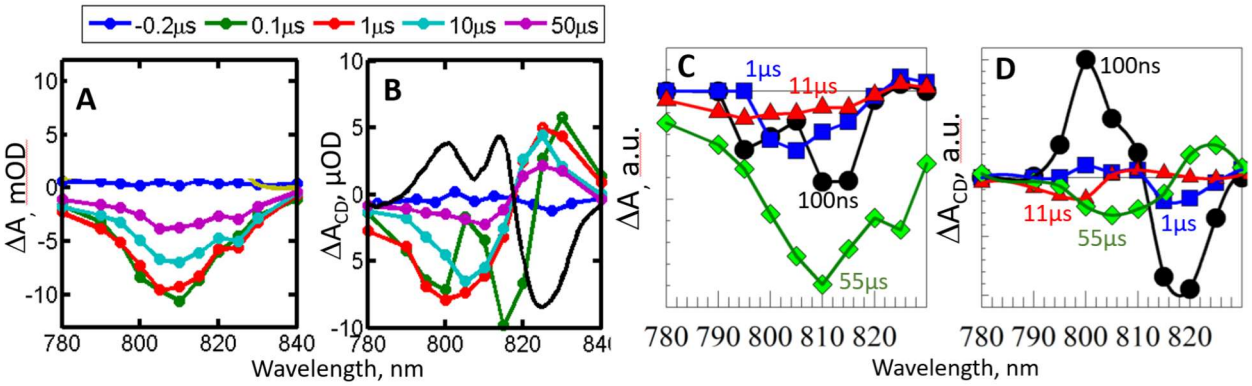

Figure 4.3(2.4.2). (**A,B**): ΔA and ΔA_{CD} differences measured at fixed times before and after excitation show rich structure in CD dynamics and little structure in ordinary absorption changes. (**C,D**): decay associated spectra reveal 4 major decay components reflecting the optical properties of individual pigments involved in the triplet energy transfer.

In Fig. 4.3A ΔA kinetics probed at a number of wavelengths (some shown in Fig. 2.1.2) are presented as spectral changes at different time delays between excitation and probe pulses. These spectra show little structure, in contrast with ΔA_{CD} shown in Fig. 4.3B. Global fit to these data reveals 4 major decay components; the respective decay associated difference spectra (DADS) for ΔA and ΔA_{CD} are shown in panels C and D.

The experimental data is analyzed in terms of the FMO Hamiltonians proposed in the past. Based on joint analysis of ΔA and ΔA_{CD} signatures, the 55 µs component is assigned to the decay of the triplet state on pigment #3, which is proposed to be the lowest energy pigment in the singlet excitation Hamiltonian in most of the successful Hamiltonians. It also suggests that pigment #3 has the lowest triplet energy. Similarly, the 1 µs component can be assigned to triplet energy transfer from pigment #4 to pigment #2. However, the 11 µs simulations using published Hamiltonians result in rather poor fits to CD, and the 100 ns component cannot be fit by any triplet energy transfer/decay sequence using otherwise successful Hamiltonians. Note that while ΔA data can be simulated using some published Hamiltonians, the accompanying measured ΔA_{CD} are not reproduced in these simulations. As an example, Fig. 4.4 shows the comparison of the measured 100-ns DADS with the simulated spectra assuming that this feature stems from the decay of the triplet state on pigment #1. The pair of pigments #1 and #2

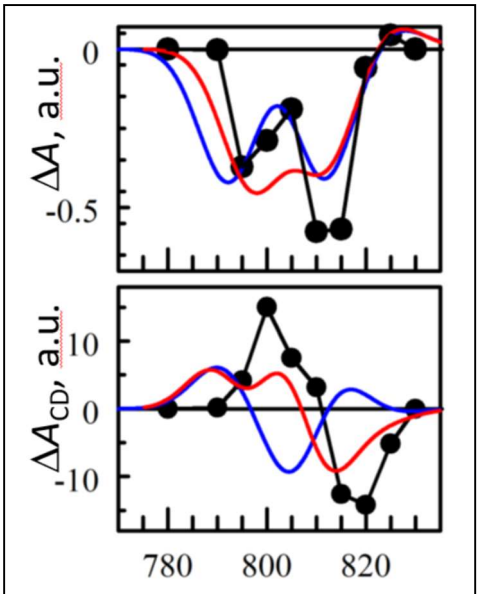

Fig.4.4. The measured 100-ns DADS (black) and simulated spectra due to triplet state decay of pigment #1 according to Hamiltonians by Brixner [1] (blue) and Kell [5] (red).

are best candidates for the strongest CD signal due to their mutual orientation and strong coupling. The blue and red curves correspond to simulations using Hamiltonians proposed by Brixner et al. [1] (based on 2D spectroscopy) and Kell et al. [5] (based on hole burning), respectively. While both Hamiltonians reproduce general shape of the ΔA signal, they predict qualitatively different CD shapes. In principle, one may tweak the diagonal energies of the two pigments in the Kell Hamiltonian to get a better fit to the 100-ns component, but due to couplings with other pigments this will have significant side effects on all other excitonic states, implying that *all* diagonal energies will need a substantial adjustment to be compatible with both past data and the new TRCD data. Additional constraints on the models are the mutual amplitudes of ΔA and ΔA_{CD}, which are unequivocally defined by the model and measured concurrently in the same time scan in experiment in absolute units.

The reasonable fits of the lower energy pigments/excitonic states using the Hamiltonians proposed earlier is not a surprise – these states are longer lived, have sharper absorption bands and thus are more easily distinguished in ultrafast time-resolved experiments (see three bands in Fig. 4.2A). The sensitivity of TRCD measurements to the higher-energy short-living excitonic states opens a unique opportunity to refine the diagonal energies of high-energy pigments in the FMO complex. While the FMO energy transfer function, in principle, could be efficient for a number of different pigment arrangements, a precise knowledge of its Hamiltonian based on experimental data makes this complex especially important for the development of theories that could predict the properties of pigment-protein complexes from *first principles*. The reasonably small size of the complex, the availability of its high-resolution structure combined with the large volume of diverse experimental data makes the FMO complex an ideal test ground for computational theory development.

To strengthen the potential of the TRCD spectroscopy in the fundamental understanding and predictive computation from *first principles* a collaboration was initiated with theory group of Prof. Slipchenko. Prof. Slipchenko is an expert in computational modeling of electronic structure in complex systems. She develops computational methodology and software for rigorous description of solute-solvent interactions with polarizable QM/MM (quantum mechanics / molecular mechanics) methods. [47-50] In these methods, a large molecular system is split in a quantum region (QM) that is described by electronic structure models for excited states such as time-dependent density functional theory (TDDFT), and a classical region (MM) that is treated with polarizable *ab initio*-based force field called the effective fragment potential (EFP). In the EFP force field all molecular parameters are obtained from a preparatory electronic structure calculation on solvent molecules (fragments) in gas phase, and do not require extensive and often ambiguous fitting to a large set of experimental or computational data.[51-54] Moreover, a functional form of the EFP force field and a functional form of the interacting QM-EFP Hamiltonian are derived from first principles and are more physically meaningful than the typically used Coulomb (based on partial charges) and van der Waals (based on R^{-6}/R^{-12}) terms of classical force fields. In polarizable models, charge distribution of the environment (protein) changes due to electric fields induced by neighboring molecular residues and electronic wave function of the QM region, and this modified charge distribution of the environment (represented by induced dipoles) talks back to the QM Hamiltonian affecting the properties of both the ground and excited states of a

chromophore. In her previous work, Slipchenko showed that QM/EFP schemes are robust in describing electronic excitations and electron ionization / attachment processes in solvated chromophores. [47, 49, 50] Recently, she extended these models for use in proteins, as well as developed fully embedded models in which the QM wave function is affected not only by Coulomb and polarization, but also van der Waals interactions with the environment. [55-57]

Our preliminary collaborative work done during this grant period shows that the polarizable QM/EFP of the FMO complex is superior to the standard QM/MM modeling and provides the correct order of the lowest pair of site energies (pigments #3 and #4), which results in qualitatively correct shapes of the low-energy parts of the absorption and CD spectra (see Fig. 4.5). This modeling gave as us a number of important insights, for example, (i) good geometries of BChl *a* pigments are essential for accurate site energies, which was achieved by constrained QM/MM optimizations of BChl *a* molecules while preserving geometry of the protein; (ii) QM region should contain not only full BChl *a* (including phytol tail) but also amino acid residues coordinating Mg centers as well as residues that are hydrogen-bonded to BChl *a*; (iii) describing BChl *a* with polarizable force field is very important as each BChl *a* induces significant solvatochromic shifts (or displacement energies) on neighboring sites, and polarization contribution to these shifts is up to 100 cm^{-1}.

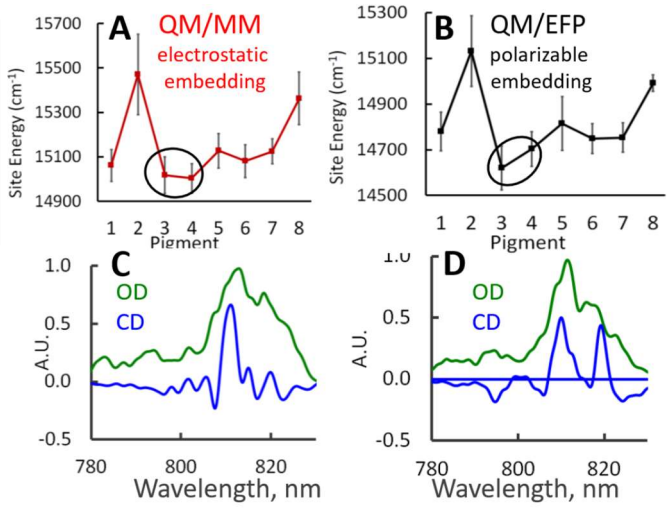

Fig.4.5. (**A,B**) Average values and standard deviations of site energies of the FMO complex (PDB ID: 3ENI) computed on a selection of 100 snapshots from molecular dynamics trajectory with QM/MM **(A)** and QM/EFP **(B)**. **(C,D)** Absorption and CD spectra computed as averages from 100 QM/MM-based (**C**) and QM/EFP-based (**D**) Hamiltonians. Polarizable protein environment in QM/EFP lowers the site energy of pigment #3, which results in qualitatively correct shapes of QM/EFP absorption and CD spectra. MD: 80 ns production run with Amber03 force field on the solvated FMO trimer structure; QM/EFP: PBE/6-31G* TDDFT. Absolute energy scales are shifted by 2750 (C) and 2400 (D) cm^{-1} to match experimental absorption maximum.

Analysis of extensive literature on modeling of the FMO complex reveals that it is extremely challenging to obtain realistic distribution of site energies (such that the Hamiltonian built on these site energies produces at least reasonable absorption and better 2DES or CD spectra) from first principles calculations without fitting parameters. [40, 58-65] While we were able to predict a quantitatively-correct order and spacing of the lowest energy sites 3 and 4, comparison of modeled and experimental CD spectra (Figs. 4.5D and 4.2A, respectively) show that the agreement in the high-energy part of the spectrum still needs to be improved. Within this proposal we will extend our initial modeling of FMO to address this and other related questions as discussed below.

Note that the nanosecond TRCD studies described above of the wild type FMO complex are in preparation for submission as a paper.

5. Additional findings during the grant period

The current grant was a continuation of a sequence of several renewal grants over a number of years. The above sections focused on the findings obtained during the last grant period that have not yet been published. Below is a brief list of earlier findings related to DOE funding, detailed information on these findings is published in open journals as listed below.

We performed comprehensive studies (published in[66]) on triplet-triplet coupling between photosynthetic pigments that involved experimental measurements of triplet exciton energies (phosphorescence spectra) in model systems and structure-based quantum mechanical modeling using Fragment Spin Difference (FSD) method. This work confirmed that FSD can reasonably well predict the triplet-triplet coupling strength between nearby pigments. The knowledge of triplet-triplet coupling is necessary to the predict possible delocalization of triplet excited states, which is necessary for proper modeling of transient ΔA_{CD} signals in the nanosecond-microsecond range.

Using 'slow' transient CD (i.e. with sub-second resolution) and structure based exciton modeling we have also investigated the electron transfer pathway in cytochrome b_6f complex [67], showing that two electrons preferentially occupy one side of the dimer, suggesting very high local dielectric constants between the low and high potential hemes of cytochrome b_6f. Similar results were obtained for the bc_1 complex [68].

In collaboration with Blankenship's group, we performed CD measurements for several site specific mutants of FMO and provided initial exciton modeling (published in [69]).

The results of the research have been routinely reported at conferences. For example, in 2018 PI presented talks at 255th ACS Meeting, 256th ACS Meeting, ISPR International Conference on Microbial Photosynthesis, 43rd Annual Midwest/Southeast Photosynthesis Meeting.

References to papers that resulted from previous DOE support

1. Xu, W., Y. Wang, E. Taylor, A. Laujac, L. Gao, S. Savikhin, P.R. Chitnis, Mutational analysis of photosystem I of Synechocystis sp. PCC 6803: the role of four conserved aromatic residues in the j-helix of PsaB. PLoS ONE, 2011. 6: p. e24625.
2. *Chauvet*, A., N. Dashdorj, J.H. Golbeck, W.T. Johnson, S. Savikhin, Spectral resolution of the primary electron acceptor A_0 in photosystem I. J. Phys. Chem. B, 2012. 116: p. 3380-3386
3. *Chauvet* A., Sarrou J, Lin S, Romberger SP, Golbeck JH, Savikhin S, Redding KE. Temporal and spectral characterization of the photosynthetic reaction center from Heliobacterium modesticaldum. Photosynth. Res. 2013, 116, p. 1-9
4. Zakharov SD, Hasan SS, Chauvet A, Savikhin S, Cramer WA. Electrostatically Constrained Pathway of Intra-Monomer Electron Transfer in the Cytochrome B6F Complex of Oxygenic Photosynthesis. Biophysical Journal. 2013 Jan 29;104(2):488a.
5. S. W. Eaton, L. E. Shoer, S. D. Karlen, S. M. , B. S. Veldkamp, C. Ramanan, D. A. *Hartzler*, S. Savikhin, T. J. Marks, M. R. Wasielewski. Singlet Exciton Fission in Polycrystalline Thin Films of a Slip-Stacked Perylenediimide. J Am Chem Soc, 2013. 135(39): p. 14701-14712.
6. Savikhin, Sergei, and Ryszard Jankowiak. "Mechanism of primary charge separation in photosynthetic reaction centers." *The Biophysics of Photosynthesis*. Springer New York, 2014. 193-

240.
7. Kihara, S., Hartzler, D.A. and Savikhin, S., 2014. Oxygen concentration inside a functioning photosynthetic cell. *Biophysical journal*, *106*(9), pp.1882-1889.
8. Hartzler DA, Niedzwiedzki DM, Bryant DA, Blankenship RE, Pushkar Y, Savikhin S. Triplet excited state energies and phosphorescence spectra of (bacterio) chlorophylls. The Journal of Physical Chemistry B. 2014;118(26):7221-32.
9. Hasan SS, Zakharov SD, Chauvet A, Stadnytskyi V, Savikhin S, Cramer WA. A Map of Dielectric Heterogeneity in a Membrane Protein: the Hetero-Oligomeric Cytochrome b_6f Complex. The Journal of Physical Chemistry B. 2014;118(24):6614-25.
10. Chauvet A, Jankowiak R, Kell A, Picorel R, Savikhin S. Does the Singlet Minus Triplet Spectrum with Major Photobleaching Band Near 680–682 nm Represent an Intact Reaction Center of Photosystem II?. The Journal of Physical Chemistry B. 2014;119(2):448-55.
11. Kihara S, Hartzler DA, Orf GS, Blankenship RE, Savikhin **S**. The Fate of the Triplet Excitations in the Fenna–Matthews–Olson Complex. The Journal of Physical Chemistry B. 2015 Apr 22;119(18):5765-72.
12. Bhaduri, S.; Stadnytskyi, V.; Zakharov, S. D.; Hasan, S. S.; Bujnowicz, Ł.; Sarewicz, M.; Savikhin, S.; Osyczka, A.; Cramer, W. A., Pathways of Transmembrane Electron Transfer in Cytochrome bc Complexes: Dielectric Heterogeneity and Interheme Coulombic Interactions. *The Journal of Physical Chemistry B* 2017**,** *121* (5), 975-983.
13. Saer, R. G.; Stadnytskyi, V.; Magdaong, N. C.; Goodson, C.; Savikhin, S.; Blankenship, R. E., Probing the excitonic landscape of the Chlorobaculum tepidum Fenna-Matthews-Olson (FMO) complex: a mutagenesis approach. *Biochimica et Biophysica Acta (BBA) - Bioenergetics* 2017**,** *1858* (4), 288-296.
14. Hartzler, D. A.; Slipchenko, L. V.; Savikhin, S., Triplet–Triplet Coupling in Chromophore Dimers: Theory and Experiment. *The Journal of Physical Chemistry A* 2018**,** *122* (33), 6713-6723.
15. Stadnytskyi, V.; Orf, G. S.; Blankenship, R. E.; Savikhin, S., Near shot-noise limited time-resolved circular dichroism pump-probe spectrometer. Review of Scientific Instruments 2018, 89 (3), 033104
16. W Xu, Y Wang, L Luo, A Chistoserdov, JH Golbeck, S Savikhin, PR Chitnis. A hydrogen bond to the A_0 chlorophyll *a* molecule of Photosystem I influences the spectral properties of A_0. To be submitted in January 2019.
17. V Stadnytskyi, G Orf, RE Blankenship, S Savikhin. Time-resolved CD spectroscopy of the Fenna Matthews Olson complex: a probe of excitonic states. To be sumbitted in February 2019.

6. Conclusion

In the last grant period, our group час developed ultrasensitive TRCD spectrometers with time resolution spanning from femtoseconds to millisecond with unprecedented sensitivity that enables to use this experimental technique for wide class of systems with relatively weak CD signatures including photosynthetic pigment-protein complexes. Our group has also extended the quantum mechanical computational theory to treat time-dependent CD signals that arise in excitonic systems in pump-probe experiments. The experimental and computational methods were successfully applied to reveal exciton structure and dynamics in the FMO complex in nanosecond time window, the femtosecond TRCD is demonstrated to be of sufficient sensitivity to study ultrafast singlet exciton dynamics in FMO.

References

1. Brixner, T.; Stenger, J.; Vaswani, H. M.; Cho, M.; Blankenship, R. E.; Fleming, G. R., Two-dimensional spectroscopy of electronic couplings in photosynthesis. *Nature* **2005,** *434* (7033), 625-628.
2. Lewis, J. W.; Tilton, R. F.; Einterz, C. M.; Milder, C. J.; Kuntz, I. D.; Kliger, D. S., New technique for measuring circular dichroism changes on a nanosecond time scale. Application to (carbonmonoxy)myoglobin and (carbonmonoxy)hemoglobin. *J Chem Phys* **1985,** *89*, 289-294.
3. Stadnytskyi, V.; Orf, G. S.; Blankenship, R. E.; Savikhin, S., Near shot-noise limited time-resolved circular dichroism pump-probe spectrometer. *Review of Scientific Instruments* **2018,** *89* (3), 033104.
4. Tronrud, D. E.; Wen, J. Z.; Gay, L.; Blankenship, R. E., The structural basis for the difference in absorbance spectra for the FMO antenna protein from various green sulfur bacteria. *Photosynthesis Research* **2009,** *100* (2), 79-87.
5. Kell, A.; Blankenship, R. E.; Jankowiak, R., Effect of Spectral Density Shapes on the Excitonic Structure and Dynamics of the Fenna–Matthews–Olson Trimer from Chlorobaculum tepidum. *The Journal of Physical Chemistry A* **2016,** *120* (31), 6146-6154.
6. Bjorling, S. C.; Zhang, C. F.; Farrens, D. L.; Song, P. S.; Kliger, D. S., Time-resolved circular dichroism of native oat phytochrome photointermediates. *Journal of the American Chemical Society* **1992,** *114* (12), 4581-4588.
7. Lewis, J. W.; Goldbeck, R. A.; Kliger, D. S.; Xie, X.; Dunn, R. C.; Simon, J. D., Time-resolved circular dichroism spectroscopy: experiment, theory, and applications to biological systems. *The Journal of Physical Chemistry* **1992,** *96* (13), 5243-5254.
8. Chen, E.; Wood, M. J.; Fink, A. L.; Kliger, D. S., Time-resolved circular dichroism studies of protein folding intermediates of cytochrome *c*. *Biochemistry* **1998,** *37* (16), 5589-5598.
9. Trifonov, A.; Buchvarov, I.; Lohr, A.; Wurthner, F.; Fiebig, T., Broadband femtosecond circular dichroism spectrometer with white-light polarization control. *Rev Sci Instrum* **2010,** *81* (4), 043104-043104-6.
10. Fidler, A. F.; Singh, V. P.; Long, P. D.; Dahlberg, P. D.; Engel, G. S., Dynamic localization of electronic excitation in photosynthetic complexes revealed with chiral two-dimensional spectroscopy. *Nature Communications* **2014,** *5*, 3286.
11. Hiramatsu, K.; Nagata, T., Communication: Broadband and ultrasensitive femtosecond time-resolved circular dichroism spectroscopy. *The Journal of Chemical Physics* **2015,** *143* (12), 121102.
12. Zhang, C.; Lewis, J.; Cerpa, R.; Kuntz, I.; Kliger, D., Nanosecond circular dichroism spectral measurements: extension to the far-ultraviolet region. *The Journal of Physical Chemistry* **1993,** *97* (21), 5499-5505.
13. Shapiro, D. B.; Goldbeck, R. A.; Che, D.; Esquerra, R. M.; Paquette, S. J.; Kliger, D. S., Nanosecond optical rotatory dispersion spectroscopy: application to photolyzed hemoglobin-CO kinetics. *Biophysical Journal* **1995,** *68* (1), 326-334.
14. Xie, X.; Simon, J. D., A picosecond circular dichroism study of photosynthetic reaction centers from Rhodobacter sphaeroides. *Biochimica et Biophysica Acta (BBA)-Bioenergetics* **1991,** *1057* (1), 131-139.
15. Mendonça, L.; Steinbacher, A.; Bouganne, R.; Hache, F., Comparative study of the folding/unfolding dynamics of poly (glutamic acid) in light and heavy water. *The Journal of Physical Chemistry B* **2014,** *118* (20), 5350-5356.

16. Anson, M.; Bayley, P., Measurement of circular dichroism at millisecond time resolution: A stopped-flow circular dichroism system. *Journal of Physics E: Scientific Instruments* **1974,** *7* (6), 481.
17. Savikhin, S., Shot-noise-limited detection of absorbance changes induced by subpicojoule laser pulses in optical pump-probe experiments. *Rev. Sci. Instrum.* **1995,** *66*, 4470-4474.
18. Savikhin, S.; Zhou, W.; Blankenship, R. E.; Struve, W. S., Femtosecond energy transfer and spectral equilibration in bacteriochlorophyll a-protein antenna trimers from the green bacterium Chlorobium tepidum. *Biophys. J.* **1994,** *66*, 110-114.
19. Savikhin, S.; Zhou, Y.; Lin, S.; Blankenship, R. E.; Struve, W. S., Femtosecond spectroscopy of Chlorosome antennas the green photosynthetic bacterium Chloroflexus aurantiacus. *J. Phys. Chem.* **1994,** *98*, 10322-10334.
20. Savikhin, S.; Struve, W. S., Ultrafast energy transfer in FMO trimers from the green bacterium Chlorobium tepidum. *Biochemistry* **1994,** *33*, 11200-11208.
21. Savikhin, S.; van Noort, P. I.; Blankenship, R. E.; Struve, W. S., Femtosecond probe of structural analogies between light-harvesting chlorosome antennae and self-assembled bacteriochlorophyll aggregates. *Biophys. J.* **1995,** *69* (3), 1100-1105.
22. Savikhin, S.; van Noort, P. I.; Zhu, Y.; Lin, S.; Blankenship, R. E.; Struve, W. S., Ultrafast energy transfer in light-harvesting chlorosomes from the green sulfur bacterium *Chlorobium tepidum*. *Chem. Phys.* **1995,** *194*, 245-258.
23. Savikhin, S.; Zhu, Y.; Blankenship, R. E.; Struve, W. S., Intraband Energy Transfers in the BChl c Antenna of Chlorosomes from the Green Photosynthetic Bacterium Chloroflexus aurantiacus. *J. Phys. Chem.* **1996,** *100* (45), 17978-17980.
24. Savikhin, S.; Struve, W. S., Low-temperature energy transfer in FMO trimers from the green photosynthetic bacterium Chlorobium tepidum. *Photosynth. Res.* **1996,** *48*, 271-276.
25. Savikhin, S.; Buck, D. R.; Struve, W. S., Toward level-to-level energy transfers in photosynthesis: the Fenna-Matthews-Olson protein (Featured Article). *J. Phys. Chem. B.* **1998,** *102*, 5556-5565.
26. van Amerongen, H.; Valkunas, L.; van Grondelle, R., *Photosynthetic excitons*. World Scientific: Singapore, 2000.
27. *Numerical recipes in C : the art of scientific computing*. Cambridge Cambridgeshire ; New York : Cambridge University Press: Cambridge [Cambridgeshire] ; New York, 1992.
28. Matthews, B. W.; Fenna, R. E.; Bolognesi, M. C.; Schmid, M. F.; Olson, J. M., Structure of a bacteriochlorophyll *a*-protein from the green photosynthetic bacterium *Prosthecochloris aestuarii*. *J Mol Biol* **1979,** *131* (2), 259-285.
29. Olson, J., The FMO protein. In *Discoveries in Photosynthesis*, Govindjee; Beatty, J. T.; Gest, H.; Allen, J., Eds. Springer Netherlands: 2005; Vol. 20, pp 421-427.
30. Milder, M. W.; Brüggemann, B.; Grondelle, R.; Herek, J., Revisiting the optical properties of the FMO protein. *Photosynth. Res.* **2010,** *104* (2-3), 257-274.
31. Savikhin, S.; Buck, D. R.; Struve, W. S., Oscillating anisotropies in a bacteriochlorophyll protein: evidence for quantum beating between exciton levels. *Chem. Phys.* **1997,** *223*, 303-312.
32. Allodi, M. A.; Otto, J. P.; Sohail, S. H.; Saer, R. G.; Wood, R. E.; Rolczynski, B. S.; Massey, S. C.; Ting, P.-C.; Blankenship, R. E.; Engel, G. S., Redox Conditions Affect Ultrafast Exciton Transport in Photosynthetic Pigment–Protein Complexes. *The Journal of Physical Chemistry Letters* **2018,** *9* (1), 89-95.
33. Fidler, A. F.; Caram, J. R.; Hayes, D.; Engel, G. S., Towards a coherent picture of excitonic coherence in the Fenna–Matthews–Olson complex. *Journal of Physics B: Atomic, Molecular and Optical Physics* **2012,** *45* (15), 154013.
34. Engel, G. S., Quantum coherence in photosynthesis. *Procedia Chemistry* **2011,** *3* (1), 222-231.
35. Blankenship, R. E.; Olson, J. M.; Miller, M., Antenna complexes from green photosynthetic bacteria. In *Anoxygenic Photosynthetic Bacteria*, Blankenship, R. E.; Madigan, M. T.; Bauer, C. E., Eds. Kluwer: Dordrecht, 1995; pp 399-435.

36. Schmidt am Busch, M.; Müh, F.; El-Amine Madjet, M.; Renger, T., The eighth bacteriochlorophyll completes the excitation energy funnel in the FMO protein. *J Phys Chem Lett* **2011,** *2* (2), 93-98.
37. Ben-Shem, A.; Frolow, F.; Nelson, N., Evolution of photosystem I – from symmetry through pseudosymmetry to asymmetry. *FEBS Letters* **2004,** *564* (3), 274-280.
38. Tronrud, D.; Wen, J.; Gay, L.; Blankenship, R., The structural basis for the difference in absorbance spectra for the FMO antenna protein from various green sulfur bacteria. *Photosynth Res* **2009,** *100* (2), 79-87.
39. Vulto, S. I. E.; de Baat, M. A.; Louwe, R. J. W.; Permentier, H. P.; Neef, T.; Miller, M.; van Amerongen, H.; Aartsma, T. J., Exciton Simulations of Optical Spectra of the FMO Complex from the Green Sulfur Bacterium Chlorobium tepidum at 6 K. *J Phys Chem B* **1998,** *102* (47), 9577-9582.
40. Olbrich, C.; Jansen, T. L.; Liebers, J. r.; Aghtar, M.; Strümpfer, J.; Schulten, K.; Knoester, J.; Kleinekathöfer, U., From atomistic modeling to excitation transfer and two-dimensional spectra of the FMO light-harvesting complex. *The Journal of Physical Chemistry B* **2011,** *115* (26), 8609-8621.
41. Adolphs, J.; Renger, T., How proteins trigger excitation energy transfer in the FMO complex of green sulfur bacteria. *Biophysical J* **2006,** *91* (8), 2778-2797.
42. Buck, D. R.; Savikhin, S.; Struve, W. S., Effect of diogonal energy disorder on circular dichroism spectra of Fenna-Matthews-Olson trimers. *J. Phys. Chem. B* **1997,** *101* (42), 8395-8397.
43. Buck, D. R.; Savikhin, S.; Struve, W. S., Ultrafast absorption difference spectra of the FMO protein at 19 K: Experiment and simulations. *Biophys. J.* **1997,** *72*, 24-36.
44. Savikhin, S.; Buck, D. R.; Struve, W. S., Pump-probe anisotropies of Fenna-Matthews-Olson protein trimers from *Chlorobium tepidum*: a diagnostic for exciton localization? *Biophys. J.* **1997,** *73*, 2090-2096.
45. Savikhin, S.; Buck, D. R.; Struve, W. S., The Fenna-Matthews-Olson protein: a strongly coupled photosynthetic antenna. In *Resonance energy transfer*, Andrews, D. L.; Demidov, A. A., Eds. John Wiley & Sons: New York, 1999; pp 399-434.
46. Kihara, S.; Hartzler, D.; Orf, G. S.; Blankenship, R. E.; Savikhin, S., The Fate of the Triplet Excitations in the Fenna-Matthews-Olson Complex and Stability of the Complex. *Biophysical Journal 106* (2), 182a.
47. Ghosh, D.; Isayev, O.; Slipchenko, L. V.; Krylov, A. I., Effect of solvation on the vertical ionization energy of thymine: from microhydration to bulk. *The Journal of Physical Chemistry A* **2011,** *115* (23), 6028-6038.
48. Gordon, M. S.; Fedorov, D. G.; Pruitt, S. R.; Slipchenko, L. V., Fragmentation methods: a route to accurate calculations on large systems. *Chemical reviews* **2011,** *112* (1), 632-672.
49. Slipchenko, L. V., Solvation of the excited states of chromophores in polarizable environment: orbital relaxation versus polarization. *The Journal of Physical Chemistry A* **2010,** *114* (33), 8824-8830.
50. Kosenkov, D.; Slipchenko, L. V., Solvent effects on the electronic transitions of p-nitroaniline: A QM/EFP study. *The Journal of Physical Chemistry A* **2010,** *115* (4), 392-401.
51. Gordon, M. S.; Freitag, M. A.; Bandyopadhyay, P.; Jensen, J. H.; Kairys, V.; Stevens, W. J., The effective fragment potential method: A QM-based MM approach to modeling environmental effects in chemistry. *The Journal of Physical Chemistry A* **2001,** *105* (2), 293-307.
52. Ghosh, D.; Kosenkov, D.; Vanovschi, V.; Flick, J.; Kaliman, I.; Shao, Y.; Gilbert, A. T.; Krylov, A. I.; Slipchenko, L. V., Effective fragment potential method in Q-CHEM: A guide for users and developers. *Journal of computational chemistry* **2013,** *34* (12), 1060-1070.
53. Gordon, M. S.; Smith, Q. A.; Xu, P.; Slipchenko, L. V., Accurate first principles model potentials for intermolecular interactions. *Annual review of physical chemistry* **2013,** *64*, 553-578.
54. Ghosh, D.; Kosenkov, D.; Vanovschi, V.; Williams, C. F.; Herbert, J. M.; Gordon, M. S.; Schmidt, M. W.; Slipchenko, L. V.; Krylov, A. I., Noncovalent interactions in extended systems described

by the effective fragment potential method: Theory and application to nucleobase oligomers. *The Journal of Physical Chemistry A* **2010,** *114* (48), 12739-12754.
55. Viquez Rojas, C. I.; Fine, J.; Slipchenko, L. V., Exchange-repulsion energy in QM/EFP. *The Journal of chemical physics* **2018,** *149* (9), 94103-94103.
56. Slipchenko, L. V.; Gordon, M. S.; Ruedenberg, K., Dispersion interactions in QM/EFP. *The Journal of Physical Chemistry A* **2017,** *121* (49), 9495-9507.
57. Gurunathan, P. K.; Acharya, A.; Ghosh, D.; Kosenkov, D.; Kaliman, I.; Shao, Y.; Krylov, A. I.; Slipchenko, L. V., Extension of the effective fragment potential method to macromolecules. *The Journal of Physical Chemistry B* **2016,** *120* (27), 6562-6574.
58. Curutchet, C.; Mennucci, B., Quantum chemical studies of light harvesting. *Chemical reviews* **2016,** *117* (2), 294-343.
59. Jurinovich, S.; Curutchet, C.; Mennucci, B., The Fenna–Matthews–Olson Protein Revisited: A Fully Polarizable (TD)DFT/MM Description. *ChemPhysChem* **2014,** *15* (15), 3194-3204.
60. List, N. H.; Curutchet, C.; Knecht, S.; Mennucci, B.; Kongsted, J., Toward reliable prediction of the energy ladder in multichromophoric systems: A benchmark study on the FMO light-harvesting complex. *Journal of chemical theory and computation* **2013,** *9* (11), 4928-4938.
61. Jia, X.; Mei, Y.; Zhang, J. Z.; Mo, Y., Hybrid QM/MM study of FMO complex with polarized protein-specific charge. *Scientific reports* **2015,** *5*, 17096.
62. Gao, J.; Shi, W.-J.; Ye, J.; Wang, X.; Hirao, H.; Zhao, Y., QM/MM modeling of environmental effects on electronic transitions of the FMO complex. *The Journal of Physical Chemistry B* **2013,** *117* (13), 3488-3495.
63. Adolphs, J.; Müh, F.; Madjet, M. E.-A.; Renger, T., Calculation of pigment transition energies in the FMO protein. *Photosynthesis research* **2008,** *95* (2-3), 197.
64. Higashi, M.; Saito, S., Quantitative Evaluation of Site Energies and Their Fluctuations of Pigments in the Fenna–Matthews–Olson Complex with an Efficient Method for Generating a Potential Energy Surface. *Journal of chemical theory and computation* **2016,** *12* (8), 4128-4137.
65. Schmidt am Busch, M.; Müh, F.; El-Amine Madjet, M.; Renger, T., The eighth bacteriochlorophyll completes the excitation energy funnel in the FMO protein. *The journal of physical chemistry letters* **2010,** *2* (2), 93-98.
66. Hartzler, D. A.; Slipchenko, L. V.; Savikhin, S., Triplet–Triplet Coupling in Chromophore Dimers: Theory and Experiment. *The Journal of Physical Chemistry A* **2018,** *122* (33), 6713-6723.
67. Hasan, S. S.; Zakharov, S. D.; Chauvet, A.; Stadnytskyi, V.; Savikhin, S.; Cramer, W. A., A Map of Dielectric Heterogeneity in a Membrane Protein: the Hetero-Oligomeric Cytochrome b6f Complex. *The Journal of Physical Chemistry B* **2014,** *118* (24), 6614-6625.
68. Bhaduri, S.; Stadnytskyi, V.; Zakharov, S. D.; Hasan, S. S.; Bujnowicz, Ł.; Sarewicz, M.; Savikhin, S.; Osyczka, A.; Cramer, W. A., Pathways of Transmembrane Electron Transfer in Cytochrome bc Complexes: Dielectric Heterogeneity and Interheme Coulombic Interactions. *The Journal of Physical Chemistry B* **2017,** *121* (5), 975-983.
69. Saer, R. G.; Stadnytskyi, V.; Magdaong, N. C.; Goodson, C.; Savikhin, S.; Blankenship, R. E., Probing the excitonic landscape of the Chlorobaculum tepidum Fenna-Matthews-Olson (FMO) complex: a mutagenesis approach. *Biochimica et Biophysica Acta (BBA) - Bioenergetics* **2017,** *1858* (4), 288-296.